Extended Higher-Order Array Decomposition Method for Fully Populated or Thinned Array Antennas and Scatterers with Connected Elements

Magnus Brandt-Møller, Michael Mattes, Olav Breinbjerg, Min Zhou and Erik Jørgensen

***Abstract*—The Higher-Order Array Decomposition Method (HO-ADM) is extended to handle fully populated or thinned finite array antennas and scatterers which can be modeled as arrays with connected elements lying on a regular lattice. The Discontinuous Galerkin Method (DGM) is employed to retain the multi-level block-Toeplitz Method of Moments (MoM) matrix structure even for connected elements. Moreover, by zeroing a selected subset of unknowns in the iterative solution process, thinned arrays can be handled as well. The presented method yields more than an order of magnitude shorter solution times for both a 32×32-element square- and a 793-element circular-thinned array with a memory consumption comparable to existing fast methods such as MLFMM.**

***Index Terms*—thinned array antennas, connected array elements, multi-level block-Toeplitz, discontinuous Galerkin method of moments, higher-order basis functions**

I. Introduction

ARRAY antennas have become a key component in numerous wireless communication and sensing applications. Phased array antennas are becoming an imperative part of next-generation space payloads and user terminals as they offer in-orbit reconfigurability and electronically steerable beams.

In order to accommodate the stringent performance requirements for space applications, future array antennas will be electrically and physically large with numerous densely packed array elements. Their performance is difficult to predict using traditional computational techniques such as embedded element patterns, primarily due to the inaccurate modeling of mutual coupling and edge effects. In addition, the larger number of needed unknowns challenges traditional full-wave numerical methods regarding memory consumption and solution time. This difficulty is further compounded when seeking an efficient solution for large finite arrays characterized by a thinned lattice, geometrically interconnected elements, and different element geometries.

For the conventional full-wave Method of Moments (MoM) for surface integral equations, the memory consumption and computational complexity scales as $\mathcal{O}(N^2)$ and $\mathcal{O}(N^2) - \mathcal{O}(N^3)$, respectively, where N is the number of unknowns. Although MoM is considered accurate in the sense that it rigorously takes into account mutual coupling and edge effects, its computational scaling is prohibitively large for the design of future electrically large but finite array antennas.

Several classes of integral-equation-based methods enable efficient full-wave analysis of electrically large arrays, in which the memory scaling and computational complexity can be reduced to as low as $\mathcal{O}(N \log N)$ by means of error-controllable approximations.

One class is the multipole-based methods such as the Multi-Level Fast Multipole Method (MLFMM) [1], [2] which is a widely used error-controllable full-wave method for electrically large structures [3], [4], [5]. Nevertheless, sub-wavelength array element sizes and spacings pose a challenge in conventional MLFMM which in addition does not exploit the typical periodic nature of arrays [6].

A second class of methods is based on MacroBasis Functions (MBFs) such as characteristic basis functions (CBF) [7], [8], synthetic basis functions (SBF) [9] and accurate subentire-domain (ASED) [10] basis functions, which are all able to drastically reduce the number of unknowns in the MoM by aggregating many elementary basis functions (BFs) into fewer groups. Nevertheless, the generation and number of MBFs to include is in general problem specific, making the asymptotic scaling difficult to predict.

A third class of methods including the fast Integral Equation Solver (IES) [11], Integral Equation QR algorithm (IE-QR) [12] and Adaptive Cross Approximation (ACA) [13] is based on lossy matrix compression. These methods can be regarded as algebraic in nature, in that they work by cleverly grouping and/or by factorization of unknowns with the aim of improving the compressibility of the system matrix and accelerating the simulation speed. Similar methods denoted as fast direct solvers are also based on compression, but focus strictly on efficient factorization and direct solution of the linear system [14], [15].

A fourth class of full-wave methods exploits the circular convolution theorem which allows the use of a Fast Fourier Transform (FFT) to accelerate the solution process. Examples are the Adaptive Integral Method (AIM) [16], [17], the pre-corrected Fast Fourier Transform method (pFFT) [18], the Integral Equation Fast Fourier Transform method (IE-FFT) [19]. In order to utilize the FFT, these methods require a regular lattice onto which the unknowns are projected.

We note that complementary methods based on the Domain Decomposition Method also allow for a very memory-efficient analysis of large finite arrays [20], [21], performing particularly well when combined with the Finite Element Method (FEM) in case of arrays with complicated stack-ups. On the other hand, integral-equation-based methods have a distinct

advantage in inherently satisfying the open boundary radiation condition, eliminating the need for less rigorous absorbing boundary conditions.

Although the above-mentioned methods employ physically and/or analytically-based approximations, most of them are error controllable, making them well-suited to accelerate the analysis of general electrically large arrays. Nevertheless, when array elements are placed on a regular lattice the computation efficiency can be improved without compromising accuracy by employing the Array Decomposition Method (ADM) [22]. The ADM exploits the translational invariance of the 3D free-space Green function in connection with the regular geometrical lattice (e.g. rectangular, hexagonal or circular) of the array elements and consecutively ordered basis functions, allowing an FFT-accelerated matrix-vector product (MVP) [22], [23] in an iterative solution process. At the penalty of approximation, the ADM can be extended using FMM, yielding $\mathcal{O}(N)$ memory consumption and a solution time which can be faster than that of ADM alone, provided that the number of far-field directions used in the basis function expansions is less than the number of unknowns on each array element [24].

Recently, the boundary integral part of ADM has been implemented with higher-order (HO) basis functions and shown to use significantly less unknowns for a given accuracy [25]. The present work concerns two further extensions to the full-wave Higher-Order Array Decomposition Method (HO-ADM) [25] for array antennas or scatterers with arbitrary perfect electrically conducting (PEC) volumetric antenna elements. In this paper, the HO-ADM is extended to allow for conduction currents between connected elements, and thus allowing for arrays with a ground-plane or other interconnecting features. A second extension is that the regular lattice does not need to be fully populated with identical array elements, hence permitting thinned arrays. The two extensions presented in this work allow for significant computational and memory savings in the HO-ADM when applied to connected and thinned arrays. This includes such challenging cases as, but not limited to, circular arrays, arrays with a finite ground-plane extending beyond the bounds of the array, and even scatterers which can be modeled as finite arrays such as a PEC plate, a cylinder, or other 2D profiles that can be extruded and modeled as an array.

The paper is organized as follows. Section II reviews the basic HO-ADM. Section III discusses the necessary extensions to HO-ADM to be able to analyze connected and thinned arrays. Section IV presents various numerical examples validating the capabilities of the extended HO-ADM. Lastly, conclusions are given in Section V. Time-harmonic variation and phasor notation is employed throughout the manuscript.

II. Higher-Order Array Decomposition Method

This section summarizes the HO-ADM [25], in which the mixed-potential electric field integral equation (EFIE), as well as the combined field integral equation (CFIE) for closed surfaces [26] have been employed.

A. Surface Discretization and Basis Functions

Curved quadrilaterals (i.e. mesh-cells), henceforth referred to as quads, with parametrization $\vec{\mathbf{r}}(u,v)$ are used to discretize the geometry [27], using the HO-hierarchical Legendre BFs from [26] to expand the surface current density as

$$\vec{\mathbf{J}}(u,v) = \frac{\vec{\mathbf{e}}_u}{\mathcal{J}_S(u,v)} \sum_{m=0}^{M^u} \sum_{n=0}^{N^v} C_{mn}^{uv} \tilde{P}_m(u) P_n(v) \alpha_{mn}^u + \frac{\vec{\mathbf{e}}_v}{\mathcal{J}_S(u,v)} \sum_{m=0}^{M^v} \sum_{n=0}^{N^u} C_{mn}^{uv} \tilde{P}_m(v) P_n(u) \alpha_{mn}^v, \quad (1)$$

in which $\{u,v\}$ are curvilinear coordinates, $\alpha_{mn}^{\{u,v\}}$ are the unknown current coefficients in the $\{u,v\}$-direction, $\vec{\mathbf{e}}_{\{u,v\}} = \frac{\partial \vec{\mathbf{r}}}{\partial \{u,v\}}$ are unitary vectors, $\mathcal{J}_S$ is the Jacobian determinant, P_n are Legendre polynomials of order n and C_{mn}^{uv} are constants chosen to minimize the MoM matrix condition number. $\tilde{P}_m$ are modified Legendre polynomials defined as

$$\tilde{P}_m(u) = \begin{cases} 1-u, & m=0 \\ 1+u, & m=1 \\ P_m(u) - P_{m-2}(u), & m \geq 2 \end{cases} \begin{matrix} \left.\vphantom{\begin{matrix}1\\1\end{matrix}}\right\} \textbf{Doublets} \\ \textbf{Singletons} \end{matrix}, \quad (2)$$

used only in the direction of the current. Herein, doublets correspond to the usual roof-top continuity-enforcing BFs having support over two quads. Singletons model local current density variations and have support only within a single quad. Other BF-formulations, e.g. Rao-Wilton-Glisson BFs on triangular cells can be used as well. Nevertheless, by using quads (instead of triangular cells) only two vectors (instead of three) are needed to represent the current, which, combined with the choice of the HO BFs in (1), enables better accuracy for the same number of unknowns [28]. In addition, since it is a hierarchical basis, the maximum polynomial order $N^{\{u,v\}} = M^{\{u,v\}} - 1$ for the current expansion in the $\{u,v\}$-direction can be chosen independently for each quad based on its electrical size.

B. Accelerated Matrix-Vector Product

For an array of antennas or scatterers with identical elements placed on a d-dimensional regular lattice, the total number of unknowns N can be formulated as

$$N = s \prod_{i=1}^{d} n_i = sT, \quad (3)$$

where s is the total number of unknowns on each array element, T is the total number of array elements and n_i is the number of elements in the i^{th} lattice dimension. Due to the translational invariance of the three-dimensional free-space Green function, the regular lattice on which array elements are placed, as well as consecutively ordered BFs, the MoM matrix $\mathbf{A} \in \mathbb{C}^{N \times N}$ becomes a multi-level asymmetric block-Toeplitz matrix of $d+1$ levels as depicted in Fig. 1b for a $T = 2 \times 3 = 6$-element array. That is, $\mathbf{A}$ consists of $n_d \times n_d$ block-Toeplitz (BT) matrices which themselves consist of $n_{d-1} \times n_{d-1}$ BT sub-blocks, and so forth for the number of array lattice dimensions d. By using the HO-hierarchical Legendre BFs

from (1), the inner-most level contains asymmetric square matrices $\mathbf{a} \in \mathbb{C}^{s\times s}$ comprising basis/test function interactions. The unknowns associated with a given array element at lattice position (a, b) is denoted as $\vec{\mathbf{x}}_{a,b}$, where $a \in \{1, \ldots, n_1\}$ and $b \in \{1, \ldots, n_2\}$.

In order to achieve an FFT-accelerated MVP, the sub-blocks at each level are extended from Toeplitz to circulant [29, sec. 4.7.7] as exemplified in Fig. 1 going from (b) $\rightarrow$ (c). The resulting extended MoM matrix, $\mathbf{A}^{\mathcal{C}}$, formally increases the number of unknowns to $\tilde{N} = s\prod_{i=1}^{d}(2n_i - 1)$, and merely serves as a mathematical trick since it does not require any zero-padding of $\mathbf{A}$ nor additional computation. This is evident from Fig. 1c, where the rearrangement of the blocks $\mathbf{a}_{k,l}$ suffices. Herein $k \in \{1, \ldots, 2n_1-1\}$ and $l \in \{1, \ldots, 2n_2-1\}$ enumerate the rearranged blocks at the first ($i = 1$) and second ($i = 2$) block-circulant level, respectively.

To ensure that the MVP with the extended MoM matrix $\mathbf{A}^{\mathcal{C}}\vec{\mathbf{x}}^{\mathcal{C}}$ contains entries equal to the original MVP, the unknown vector $\vec{\mathbf{x}} \in \mathbb{C}^{N\times 1}$ is extended to $\vec{\mathbf{x}}^{\mathcal{C}} \in \mathbb{C}^{\tilde{N}\times 1}$ as illustrated in Fig. 1c. Zeroes are placed at the positions pertaining to the extended blocks, i.e. $\vec{\mathbf{x}}_{k,l} = 0$ for $k > n_1 \wedge l > n_2$. The MVP $\mathbf{A}^{\mathcal{C}}\vec{\mathbf{x}}^{\mathcal{C}}$ favorably becomes a discrete circular block convolution operation which can be accelerated via the FFT.

In conclusion, the computational complexity of the HO-ADM becomes $\mathcal{O}(s^2T)$ in setup time and $\mathcal{O}(s^2T\log(T))$ for the MVP. The memory consumption is $\mathcal{O}(s^2T)$. Note that the quadratic scaling with s is a consequence of permitting a general matrix $\mathbf{a}_{k,l}$ at the inner most level. Nevertheless, by employing the HO-hierarchical BFs, s can be kept low (compared to ordinary first-order BFs) without impacting the solution accuracy [25].

III. Extended Array Decomposition Method

In the existing HO-ADM no conduction current is allowed to flow between adjacent array elements, effectively excluding arrays with a ground-plane or other interconnecting features. Another restriction is that the regular d-dimensional lattice has to be fully populated with identical array elements. In this section two contributions to the existing HO-ADM are presented enabling it to handle electrically connected and thinned arrays. From this point, HO-ADM will refer to the extended method.

A. Extension to Thinned Arrays

Thinned array antennas are obtained by terminating or removing elements from uniformly spaced arrays [30]. The main motivation for thinning array antennas is the achievable reduction in cost and weight, without compromising desired performance parameters such as gain, beamwidth, or side lobe level. Another incentive for thinning can be spatial constraints, where the outer elements in a regular array need to be removed to conform to a given rim. In the remainder of this paper, the term thinning will refer to the removal of elements.

The challenge in retaining an FFT-accelerated MVP, when array elements are removed, is that the multi-level block-Toeplitz (MBT) property of the system matrix is lost. The

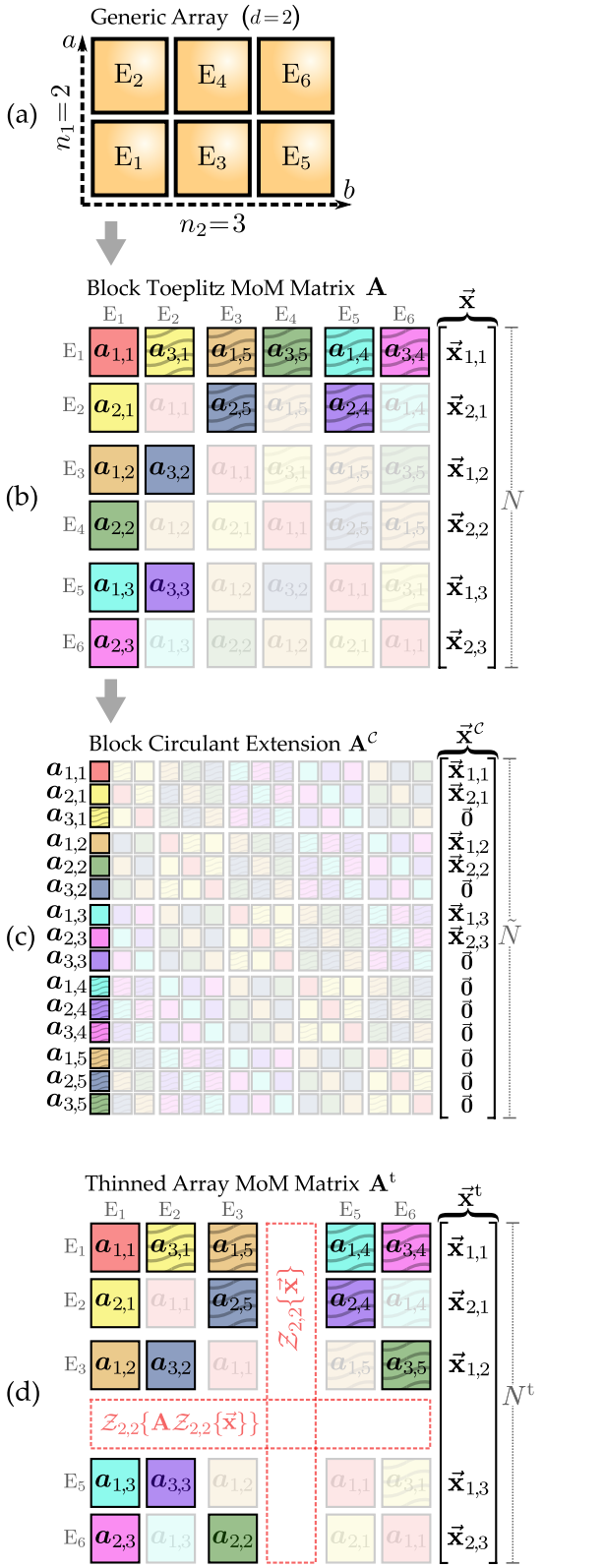

Fig. 1: Example of (a) $T = 2\times 3 = 6$-element generic array, (b) the resulting multi-level block Toeplitz MoM matrix $\mathbf{A}$ with $N = sT$ unknowns, (c) its full circulant extension $\mathbf{A}^{\mathcal{C}}$ with $\tilde{N} \approx 2^d N$ unknowns and (d) the thinned MoM matrix $\mathbf{A}^{\mathrm{t}}$ after removing element four (E_4). Colors indicate similar interaction matrices, while faint colors indicate blocks that do not need to be computed nor stored. A wavy pattern indicates blocks that have to be computed if the employed integral operators are not symmetric. In case of symmetric operators their calculation can be omitted.

thinned MoM matrix $\mathbf{A}^{\mathrm{t}} \in \mathbb{C}^{N^{\mathrm{t}} \times N^{\mathrm{t}}}$ results in the reduced system

$$\mathbf{A}^{\mathrm{t}} \vec{\mathbf{x}}^{\mathrm{t}} = \vec{\mathbf{b}}^{\mathrm{t}}, \tag{4}$$

where $\vec{\mathbf{x}}^{\mathrm{t}} \in \mathbb{C}^{N^{\mathrm{t}} \times 1}$ is the resulting thinned unknown vector, $\vec{\mathbf{b}}^{\mathrm{t}} \in \mathbb{C}^{N^{\mathrm{t}} \times 1}$ is the thinned right-hand side, and N^{t} is the total number of unknowns after thinning the array. Fig. 1d shows an example where the removal of array element number four (E_4) and its associated unknowns $\vec{\mathbf{x}}_{2,2}$ results in the deletion of both a block-row and -column which in turn destroys the MBT structure.

Instead of removing elements from $\mathbf{A}$, one remedy to maintain the MBT structure is to keep $\mathbf{A}$ as is, but employ zeroing of the unknown vector and the MVP result. Herein the full length of the unknown and right-hand side vectors is retained, while the unknowns and MVP entries associated with removed elements are forced to zero. Mathematically, the MVP for the thinned system can be formulated as

$$\mathbf{A}^{\mathrm{t}} \vec{\mathbf{x}}^{\mathrm{t}} = \mathcal{Z}_{a,b}\{\mathbf{A}\mathcal{Z}_{a,b}\{\vec{\mathbf{x}}_i\}\}, \tag{5}$$

where $\mathcal{Z}_{a,b}$ is a zeroing function placing zeros at those positions (a, b) in the vector which pertains to the removed array element(s) and $\vec{\mathbf{x}}_i \in \mathbb{C}^{N \times 1}$ is the i^{th} iteration solution vector guess. Because $\mathcal{Z}_{a,b}\{\vec{\mathbf{x}}_i\}$ is of full length N, it can be multiplied on the full MoM matrix $\mathbf{A}$ possessing the MBT property, effectively preserving the FFT-acceleration.

The zeroing of unknowns pertaining to e.g. element number four (E_4) via $\mathcal{Z}_{2,2}\{\vec{\mathbf{x}}_i\}$, being equivalent to $\vec{\mathbf{x}}_{2,2} = 0$, effectively removes the influence of the blocks in column number four as illustrated with the vertical red dashed rectangle in Fig. 1d. From an electromagnetic perspective, zeroing basis function coefficients $\mathcal{Z}\{\vec{\mathbf{x}}_i\}$ in each iteration can be interpreted as enforcing zero current flow on removed element(s). Remark, however, that this does not eliminate the corresponding block-row number four, which represents the coupling from all other elements to the removed element. Therefore, to also remove the influence of the row, the MVP result $\mathbf{A}\mathcal{Z}_{2,2}\{\vec{\mathbf{x}}_i\}$ should be zeroed as well, as indicated with the horizontal red dashed rectangle in Fig. 1d.

In addition, the right-hand side vector $\vec{\mathbf{b}}$ must be zeroed accordingly in order for the iterative solver to calculate the correct residual vectors $\vec{\mathbf{r}}_i$, that is

$$\vec{\mathbf{r}}_i = \mathcal{Z}_{a,b}\{\vec{\mathbf{b}}\} - \mathcal{Z}_{a,b}\{\mathbf{A}\mathcal{Z}_{a,b}\{\vec{\mathbf{x}}_i\}\}. \tag{6}$$

Zeroing the resulting MVP, i.e. $\mathcal{Z}\{\mathbf{A}\mathcal{Z}\{\vec{\mathbf{x}}_i\}\}$, can be understood as not letting the coupling field from all other elements induce any current on the removed element(s). In short, by appropriately zeroing, the iterative solver will converge to the same solution as if the ordinary MVP $\mathbf{A}^{\mathrm{t}}\vec{\mathbf{x}}^{\mathrm{t}}$ was applied for the truncated system.

B. Extension to Electrically Connected Arrays

The MBT property of $\mathbf{A}$ is lost in the case of electrically connected array elements. This is because the doublet basis function coefficients α_{0n}, α_{1n} on connected edges have to be associated with either one or the other array element. In order to overcome this limitation, the Discontinuous Galerkin Method (DGM) for surface integral equations is employed [31].

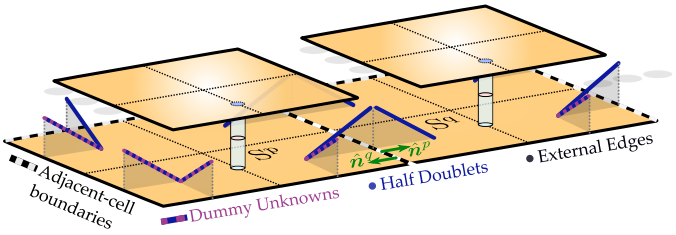

Fig. 2: Two patch elements at the corner of a larger ground-plane-connected array. Half-doublet BFs are introduced on either side of the boundaries between adjacent elements. Dummy unknowns, which are appropriately placed half-doublets, are added on external edges to retain the MoM matrix MBT property (see Section III-B2).

1) Discontinuous Galerkin Method: The DGM is commonly recognized for its ability to handle non-conformal meshes of complex targets comprising mesh elements of a wide range of electrical sizes, resulting in a significant reduction in memory consumption and solution time [32], [33], [34]. In the present contribution yet another application of the DGM is presented to retain the MBT MoM matrix $\mathbf{A}$. Quite recently, the DGM has been applied to finite array analysis [10], but not in the context of retaining the MBT property of the MoM matrix to facilitate the use of an FFT-accelerated MVP.

The essence of DGM is that current continuity is weakly enforced via an extra surface integral penalty term albeit at the cost of an increased condition number of $\mathbf{A}$ [31]. For this reason, it was proposed in [31] to stabilize the resulting DGM MoM matrix and provide practical iterative convergence with an extra boundary interior penalty stabilization function $\mathcal{I}_{\mathrm{IP}}(\beta)$

$$\mathcal{I}_{\mathrm{IP}}(\beta) = \frac{\beta}{k^2} \int_{\mathcal{C}_{pq}} [\hat{\boldsymbol{n}}^p \cdot \vec{\mathbf{f}}_t^{\,m}(\vec{\mathbf{r}})][\hat{\boldsymbol{n}}^q \cdot \vec{\mathbf{f}}_b^{\,n}(\vec{\mathbf{r}})] d\vec{\mathbf{r}}, \tag{7}$$

in which $\beta = \frac{1}{10h}$ is a scalar depending on the average electrical mesh size h, k is the wavenumber, $\vec{\mathbf{f}}_t^{\,m}$ is the m^{th} test function, $\vec{\mathbf{f}}_b^{\,n}$ is the n^{th} basis function and $\vec{\mathbf{r}}$ is a position vector along the common edge $\mathcal{C}_{pq}$ between quads p and q with in-plane outward normal unit vectors denoted as $\hat{\boldsymbol{n}}^p$ and $\hat{\boldsymbol{n}}^q$, respectively (see Fig. 2).

In the HO-ADM, exclusion of this interior boundary penalty term is paramount because including it destroys the MBT property of $\mathbf{A}$. This is due to the opposite signs of the two normal vectors $\hat{\boldsymbol{n}}^{\{p,q\}}$ when evaluated along the common edge $\mathcal{C}_{pq}$. Note that $\mathcal{I}_{\mathrm{IP}}$ is merely responsible for stabilization and that its exclusion is feasible provided proper preconditioning is employed [35], [36], [33].

2) Application of DGM in HO-ADM: With the DGM at hand, Fig. 2 illustrates how the above outlined approach is only applied at the electrically connected boundaries between array elements. More specifically, the half-doublet BFs are placed only at edges associated with two quads which lie on two different array elements. As a consequence, twice the number of doublet unknown coefficients are introduced, but only at those edges which connect different array elements.

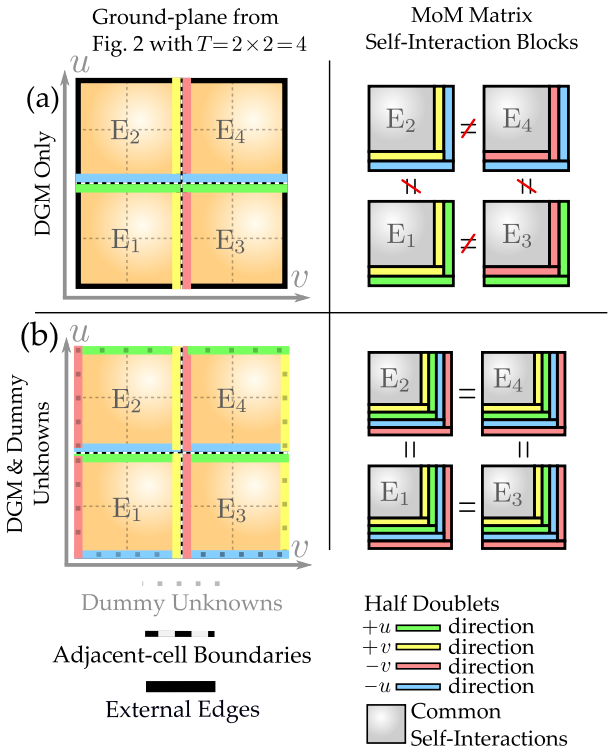

Fig. 3: Ground-plane of the array from Fig. 2 using, for illustration, $T = 2 \times 2 = 4$ elements with (a) DGM applied at differently oriented connected edges resulting in dissimilar MoM matrix self-interaction blocks and (b) with dummy BFs (half-doublets) appropriately placed at external edges in order to make self-interaction blocks equal. In this way, the full MoM matrix $\mathbf{A}$ retains its multi-level block Toeplitz property.

In the case of the patch array in Fig. 2, this means that DGM only has to be applied at the ground-plane edges. Note that this allows for normal divergence-conforming and inherently continuity-enforcing BFs between all other quads inside the array-elements.

Hence, by the use of half-doublets, the basis function coefficients can be distributed evenly between array element matrices $\mathbf{a}_{k,l}$ in $\mathbf{A}$, while the DGM maintains current continuity. The MoM matrix is, however, not yet fully BT because the array elements do not possess the same amount nor the same enumeration of BFs. Since DGM only needs to be applied at edges which connect different array elements, we focus now only on the ground-plane of the patch array of Fig. 2, which is illustrated in Fig. 3 for clarity reasons. Herein, the DGM has been used to place half-doublets on each of the connecting edges on the ground-plane between the four array elements. However, because these half-doublets are placed at differently oriented edges (indicated with colors), the resulting MoM self-interaction matrix blocks are no longer equal, despite having many basis function self-interactions in common (indicated in gray). Consequently, retaining the MBT property of $\mathbf{A}$ is not possible with the DGM alone.

3) Dummy Unknowns: To this end, a number of dummy BFs need to be added to the ground-plane on those array elements which are placed along the edges of the array. Here, one solution is to introduce half-doublets on all external edges, i.e. edges which are only associated with one quad, as illustrated in Fig. 3b. By doing so, self-interaction blocks for all array elements become equal, and the MBT property of $\mathbf{A}$ can be retained. Note that unlike the formally added unknowns $\tilde{N}$ due to the circulant extension, the additional dummy unknowns involve some overhead since they have to be computed and stored. Therefore, in the HO-ADM only strictly necessary external edges are identified on which dummy unknowns have to be placed.

Although the addition of dummy unknowns together with the DGM retains the MBT MoM matrix, the additional unknowns placed at external edges alter the Krylov subspace and subsequently the obtainable solution. It is therefore of paramount importance to exclude dummy basis function coefficients from the iterative solver. Fortunately, the technique of Section III-A can also be employed here to effectively hide dummy unknowns from the iterative solver's perspective, such that the underlying Krylov subspace remains unchanged. As such, dummy unknowns are never solved for and merely serve to preserve the MBT property of $\mathbf{A}$ for retaining a fast MVP.

After employing the DGM and adding required dummy unknowns, the total number of unknowns $N_\dagger$ can be approximated as

$$N_\dagger = [s + \kappa(s)]\, T, \tag{8}$$

where $\kappa(s) \in \{0, \ldots, s\}$ is the average number of BFs connecting two array elements. For example, if half of the BFs on an array element is electrically connected to a neighboring element $\left(\text{i.e. } \frac{\kappa(s)}{s} = 0.5\right)$, we would need 50 % more unknowns. Nevertheless, for practical antenna arrays the amount of connected edges and thus doublet BFs between array elements is considerably smaller than the number of BFs on each array element (i.e. $\kappa(s) \ll s$), hence $N_\dagger \approx N$.

In summary, by employing half-doublets only at connected boundaries between array elements (i.e. only on the ground-plane for the patch array of Fig. 2), using the DGM to enforce current continuity and by introducing dummy unknowns which are hidden from the iterative solver, electrical conduction currents are allowed to flow between array elements while retaining the MBT property of the MoM matrix, permitting an FFT-accelerated MVP.

C. Required Preconditioning Strategy

In this section, a necessary preconditioning strategy is presented in order to arrive at an effective solver for the HO-ADM in the case of connected arrays. A left-preconditioned linear system of equations is assumed, with a relative error ϵ defined as

$$\epsilon = \frac{\left\| \mathcal{P}^{-1} \left[\vec{\mathbf{b}} - \mathbf{A}\vec{\mathbf{x}}_i \right] \right\|_2}{\left\| \mathcal{P}^{-1} \vec{\mathbf{b}} \right\|_2}, \tag{9}$$

in which $\mathcal{P}$ represents a block-diagonal (BD) preconditioning matrix with ($\mathcal{P}_\text{C}$) or without ($\mathcal{P}_\text{NC}$) coupling terms from nearby array elements. Note that $\mathcal{P}$ is never formed explicitly nor applied to $\mathbf{A}$ directly.

Due to the inherent MBT structure of $\mathbf{A}$, a constant-memory block-diagonal preconditioner has been shown to be effective

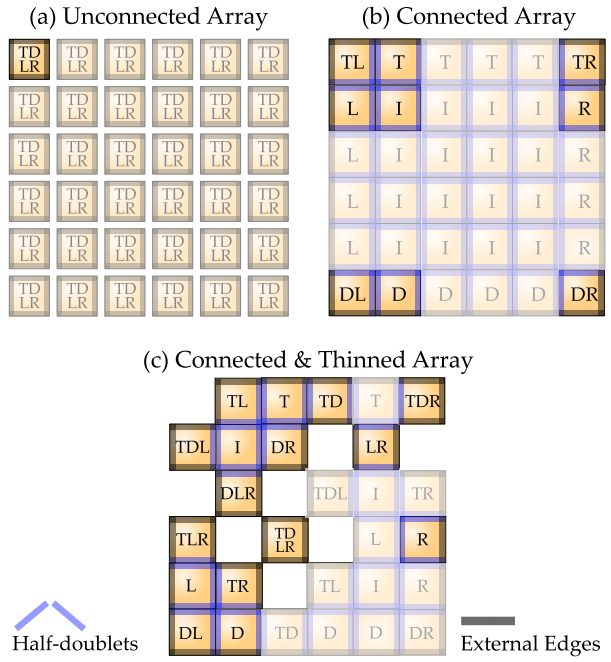

Fig. 4: Unique interaction groups required to build the constant memory NF-coupling preconditioner for the example of a 6×6 element (a) unconnected array (b) connected array and (c) connected and thinned array. DGM half-doublet BFs are placed at connected edges marked in blue. Faint colors indicate groups that do not need to be computed nor stored.

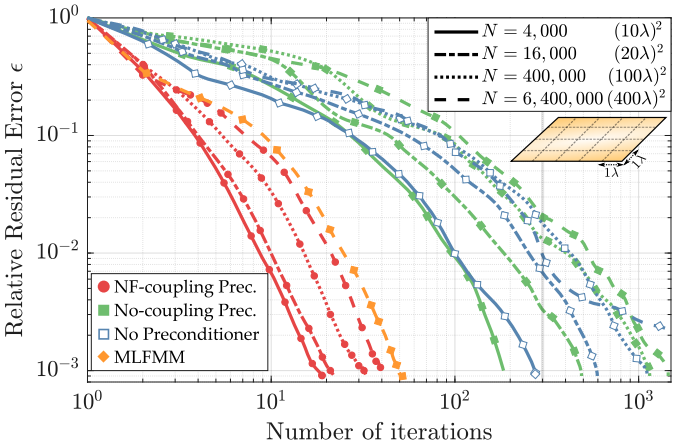

Fig. 5: Performance of the constant memory NF-coupling (CNF) preconditioner compared to the common block-diagonal preconditioner without coupling; both applied to the case of a normal-incident plane wave on ground-planes (PEC square plates) of different sizes which are constructed by electrically connecting $(1\lambda)^2$ quadrilateral mesh cells using HO-ADM. The wavelength is fixed to 1.0 m and the size is varied. For reference, the MLFMM result is presented only for the computationally most demanding case of the $(400\lambda)^2$ plate.

for the Array Decomposition Method [22]. Herein, an LU-factorization of the interaction matrix of a single array element is used in a BD preconditioner, which will be referred to as $\mathcal{P}_{\text{NC}}$. However, in the case of connected arrays in the HO-ADM, a preconditioner not including coupling with nearby array elements no longer suffices. This is mainly due to the now closely coupled half-doublet BFs but also due to the excluded interior stabilization term $\mathcal{I}_{\text{IP}}$.

1) Constant-Memory NF-Coupling Preconditioner: To overcome the bad iterative convergence when array elements become electrically connected, a NF-coupling BD preconditioner, $\mathcal{P}_{\text{C}}$, is needed. Nevertheless, an inherent challenge with BD preconditioners including coupling is that each block along the main diagonal has to be stored. For the HO-ADM, doing so would mean that the preconditioner memory consumption would become proportional to the number of array elements T and even comparable to the storage of the unique interaction matrices $\mathbf{a}_{k,l}$. However, in case of regular arrays a unique set of basis function preconditioner groups can be identified as depicted in Fig. 4 for the example of an unconnected, connected and simultaneously thinned and connected 6×6 element array.

In the simple case where elements are not electrically connected, only one interaction group, comprising the self-interactions of a single array element, needs to be computed and stored as illustrated in Fig. 4a. This corresponds to the previously discussed no-coupling preconditioner $\mathcal{P}_{\text{NC}}$. By realizing that redundant groups exist for connected arrays as well, we have in practice only nine unique preconditioner groups [I, T, D, L, R, TL, TR, DL, DR] as illustrated in Fig. 4b, in which letters {(I)nner, (T)op, (D)own, (L)eft, (R)ight} are used to distinguish unique interaction groups, and simultaneously indicate the positions of external edges for a given group. If we, in addition, allow array thinning, we can still identify a finite but slightly larger set of 16 unique preconditioner groups for a rectangular lattice as seen in Fig. 4c. Consequently, it is possible to construct a constant-memory NF-coupling (CNF) preconditioner $\mathcal{P}_{\text{C}}$ for simultaneously connected and thinned arrays, by only computing and storing at most 16 unique interaction matrices.

The CNF preconditioner $\mathcal{P}_{\text{C}}$ is constructed by LU-factorization of at most 16 unique interaction matrices, whereafter they can be applied in parallel on the complete array by simple forward/backward substitutions on the associated right-hand side ($\vec{\mathbf{b}}$) entries. Remark that building the required preconditioner groups (including coupling) requires no recomputation since all interaction information is already contained in the storage of $\mathbf{a}_{k,l}$.

In Fig. 5, the relative residual error versus the number of iterations is plotted, for comparison purposes, for the simple case of plane-wave scattering from a ground-plane (i.e. square PEC plate) of various electrical sizes modeled by connecting many smaller $(1\lambda)^2$-sized plates, where λ is the wavelength. For ground-plane sizes up to around $(100\lambda)^2$, the no-coupling preconditioner $\mathcal{P}_{\text{NC}}$ converges similarly as the system without preconditioning. For a $(400\lambda)^2$-ground-plane comprising 6.4 million (M) unknowns, the no-coupling preconditioner converges to a residual error of 10^{-3} after 1448 iterations, whereas no preconditioning stagnates at over 3200 iterations. Interestingly, it is noted that for all considered ground-plane sizes ranging from $(10\lambda)^2$ to $(400\lambda)^2$, the residual error starts out being significantly higher with the no-coupling preconditioner compared to not applying a preconditioner at all. Only for small ground-planes, e.g. $(10\lambda)^2$ and $(20\lambda)^2$, is the final number of iterations of the no-coupling preconditioner better than not applying any preconditioning. This impeded effectiveness of $\mathcal{P}_{\text{NC}}$ makes sense if we perceive the connected

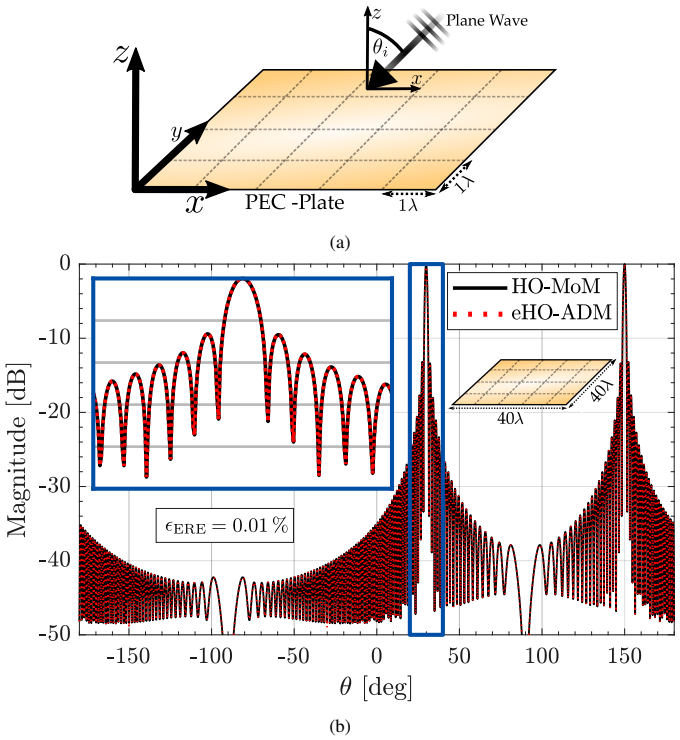

Fig. 6: Normalized scattered far-field $\phi = 180°$-cut for an obliquely incident ($\theta_i = 30°, \phi_i = 0°$) plane wave on a $(40\lambda)^2$-sized PEC square plate comparing the HO-ADM and HO-MoM. The blue marking is a view of the range $\theta = [20°, 40°]$ with the same y-axis dynamic-range as the full plot.

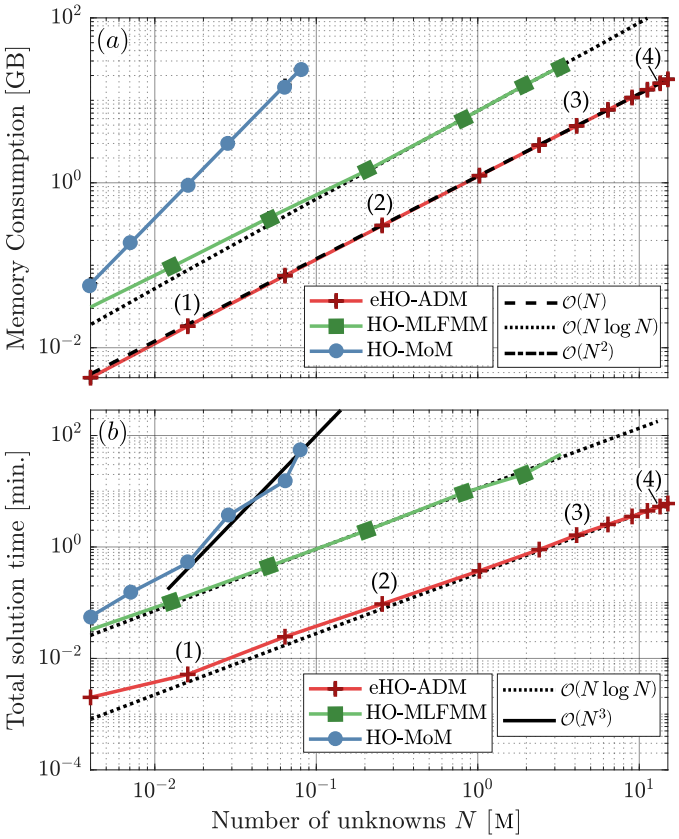

Fig. 7: Comparing HO-ADM with HO-MLFMM/HO-MoM in terms of (a) total memory consumption and (b) total solution time for the case of obliquely-incident ($\theta_i = 30°$) plane-wave scattering of various electrically large PEC plates (up to an area of $(620\lambda)^2$ corresponding to ca. 15 million unknowns). – The wavelength is fixed to 1.0 m and the size is varied. Markers do not reflect number of data points.

array using DGM as the limiting case of unconnected array elements moving closer to each other, since $\mathcal{P}_{\mathrm{NC}}$ effectively assumes an uncoupled array problem.

Instead, by applying the NF-coupling preconditioner $\mathcal{P}_{\mathrm{C}}$, a residual error of 10^{-3} is reached after 17 iterations for a $(10\lambda)^2$-ground-plane compared to 185 iterations for the simple $\mathcal{P}_{\mathrm{NC}}$ preconditioner. The efficacy is even clearer for the larger $(400\lambda)^2$-ground-plane for which the number of iterations reduces from 1448 to 41 iterations by employing $\mathcal{P}_{\mathrm{C}}$. For reference, comparison with a HO-MLFMM implementation which converges after 51 iterations for the $(400\lambda)^2$-ground-plane establishes the efficacy of $\mathcal{P}_{\mathrm{C}}$. Here it should be stressed that the HO-MLFMM implementation also employs a coupling preconditioner and that HO-MLFMM uses a flexible generalized minimal residual (GMRES) solver including inner and outer iterations. Therefore, to make a fair comparison with HO-MLFMM, only outer iterations have been allowed.

IV. Validation Examples

Numerical experiments are performed to demonstrate the validity and efficiency of the presented HO-ADM. Results have been generated on a computer with an Intel® Core® i7-9850H CPU @ 2.6 GHz with 6 cores and 32 GB of RAM, unless otherwise stated. The GMRES iterative solver is employed with Krylov subspace maximum dimension of 300 and relative residual error tolerance of 10^{-3}. Comparisons are made with the full-wave solver in ESTEAM [37] which is based on a state-of-the-art HO-MoM/MLFMM implementation [26], [38]. In the following, total solution time includes the generation of BFs, the calculation of and the block-FFT across unique interaction blocks, the preconditioner generation, and the iterative solution time. Total memory consumption refers to the storage of required matrices, the Krylov subspace, as well as the preconditioner. An Equivalent Relative Error (ERE) is used to compare HO-ADM with HO-MLFMM

$$\epsilon_{\mathrm{ERE}} = \sqrt{\frac{\sum_{i=1}^{N_s} |\mathbf{E}_{i,\mathrm{ADM}} - \mathbf{E}_{i,\mathrm{MoM/MLFMM}}|^2}{\sum_{i=1}^{N_s} |\mathbf{E}_{i,\mathrm{MoM/MLFMM}}|^2}}, \tag{10}$$

where $\mathbf{E}_{\mathrm{ADM}}$ and $\mathbf{E}_{\mathrm{MoM/MLFMM}}$ are the electric far-field vectors for HO-ADM and HO-MoM/MLFMM, respectively. $N_s = 5403$ is the number of far-field samples used on a regular θ-ϕ-grid over the 4π far-field sphere for the examples of Section IV.

A. Plane Wave Incidence on Square Plate

As a first validation example, we continue the example of the ground-plane of Fig. 5 and consider the problem of a plane wave obliquely incident ($\theta_i = 30°, \phi_i = 0°$) on a square $(40\lambda)^2$-sized PEC plate, as depicted in Fig. 6a. The scattered far-field is plotted in Fig. 6b for a $\phi = 180°$-cut and is seen to coincide with the results of the HO-MoM within the full dynamic range (50 dB) with an equivalent relative error of

TABLE I: Total solution time and memory consumption samples from Fig. 7 for ground-planes of various sizes, comparing HO-MLFMM and HO-ADM on an Intel® Core® i7-9850H CPU @ 2.6 GHz with 6 cores. Note that separating s and T ($N = sT$) is only valid for HO-ADM.

Ground-plane Size	HO-MLFMM				HO-ADM				
	Time	Mem.	N	Iter.	Time	Mem.	s	T	Iter.
1: $(10\lambda)^2$	1.5 s	25 MB	3120	11	0.1 s	4.4 MB	40	100	18
2: $(80\lambda)^2$	118 s	1.4 GB	204,160	17	5.7 s	0.3 GB	40	6400	29
3: $(320\lambda)^2$	46 m	26 GB	3,274,240	28	98 s	4.9 GB	40	102400	40
4: $(620\lambda)^2$	-	90 GB	12,300,800	-	6 m	18 GB	40	384400	53

$0.01\,\%$. In the HO-ADM, the plate is modeled as many $(1\lambda)^2$-sized connected elements (see Fig. 6a) and by applying the DGM with dummy unknowns as described in Section III-B.

In Fig. 7 the total solution time and memory consumption is plotted, including theoretical asymptotic scaling, comparing HO-MoM/MLFMM and the HO-ADM for increasingly larger plates. Note that the wavelength is fixed to $1.0\,\mathrm{m}$ and the size is varied. Selected samples (marked with numbers in parenthesis in Fig. 7) have been tabulated in Table I. Herein it is evident that HO-ADM is more than an order of magnitude faster than the HO-MLFMM in terms of total solution time in the whole span from $N = 4,000$ to $N = 15\,\mathrm{M}$ unknowns. For PEC plates smaller than $(80\lambda)^2$ corresponding to $N = 256,000$ unknowns, the total solution time of the HO-ADM does not follow the theoretical asymptotic scaling because it is dominated by the overhead associated with the special DGM and dummy unknowns handling.

For a larger $(320\lambda)^2$ PEC plate, the HO-ADM requires circa $N = 4\,\mathrm{M}$ unknowns and uses $98\,\mathrm{s}$ with $5\,\mathrm{GB}$ of total memory consumption whereas MLFMM requires around $N = 3.2\,\mathrm{M}$ unknowns but uses $46\,\mathrm{min}$ with a memory consumption of $26\,\mathrm{GB}$. For the largest $(620\lambda)^2$ PEC plate ($N \approx 15\,\mathrm{M}$), HO-ADM uses a total simulation time of around $6\,\mathrm{min}$, and a memory consumption of $18\,\mathrm{GB}$, whereas HO-MLFMM would require $90\,\mathrm{GB}$ and could not be run on the computer at hand.

B. Phased Patch Antenna Array

As a second example, we consider a 32×32-element dual-frequency right-hand circularly polarized (RHCP) high-gain antenna array based on the design from [39] with 1024 independent wire excitations, which is illustrated in Fig. 8a including the employed simulation mesh. The array is meshed with a total of $122{,}880$ quadrilaterals comprising $N \approx 975{,}000$ unknowns in the HO-MLFMM, whereas $N \approx 1\,\mathrm{M}$ unknowns are needed in the HO-ADM due to the DGM and dummy unknowns as described in Section III-B.

The radiated far-field pattern in Fig. 9a has been computed at $8.4\,\mathrm{GHz}$, and the peak directivity for both HO-ADM and HO-MLFMM is $38.4\,\mathrm{dBi}$ (which is close to the reported calculated directivity of $38.5\,\mathrm{dBi}$ [39] considering that not all design parameters are known). In Fig. 9a both the co- and cross-polarization patterns are seen to coincide comparing the HO-ADM with HO-MLFMM, with an equivalent relative error of $0.03\,\%$ and $0.05\,\%$ for co-pol and cx-pol, respectively.

Table II shows a comparison of solution time and memory consumption between the HO-ADM and ESTEAM. For HO-

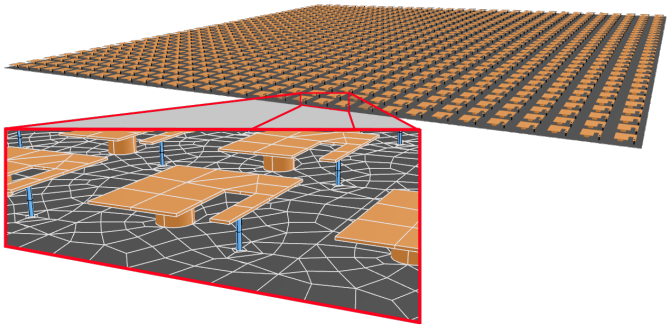

(a)

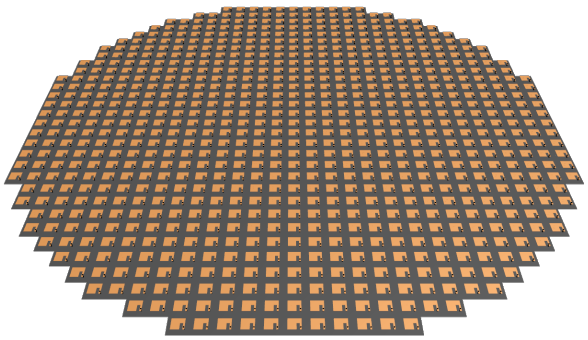

(b)

Fig. 8: (a) 32×32-element dual-frequency right-hand circularly polarized all-metal high-gain antenna array, including employed meshing of the element cell for the reported results. – White lines indicate edges of the mesh, blue signify wire-quads, dark gray quads designate the ground-plane and orange illustrate quads on the radiating elements. (b) Thinned 793-element all-metal array conforming to a circular rim.

TABLE II: Total solution time and memory consumption for the 32×32 array in Fig. 8a and the corresponding circular-thinned array in Fig. 8b, comparing HO-MLFMM and HO-ADM on an Intel® Core® i9-10980XE CPU @ 3.0 GHz with 18 cores. Results in parentheses are for the thinned array.

Method	Total Simulation Time	Memory Consumption	Number of Iterations	Time per Iteration
HO-MoM	N/A	3540 GB	N/A	N/A
HO-MLFMM	1 h 2 min	25.1 GB	540	3.9 s
	(57 min)	(22.5 GB)	(567)	(3.8 s)
HO-ADM	6 min 18 s	28.2 GB	481	0.4 s
	(6 min 18 s)	(28.2 GB)	(506)	(0.38 s)

MLFMM the solution time is around 1 hour with a memory consumption of only $25.1\,\mathrm{GB}$. At the penalty of slightly increased memory consumption ($28.2\,\mathrm{GB}$) using the extended HO-ADM, the solution time can be reduced by a factor of 10 to around 6 min. Both HO-MLFMM and HO-ADM use around half of the total solution time to setup matrices and the other half to solve the system, and both use approximately the same order of iterations. The ten-fold reduction in solution time for HO-ADM is observed both in terms of setup time and time per iteration.

Whereas a speed-up by a factor of 30 is possible in the case of an electrically large PEC plate constructed by simple flat quads, a speed-up by a factor of only 10 is achievable for the 32×32 array. The main reason is the quadratic com-

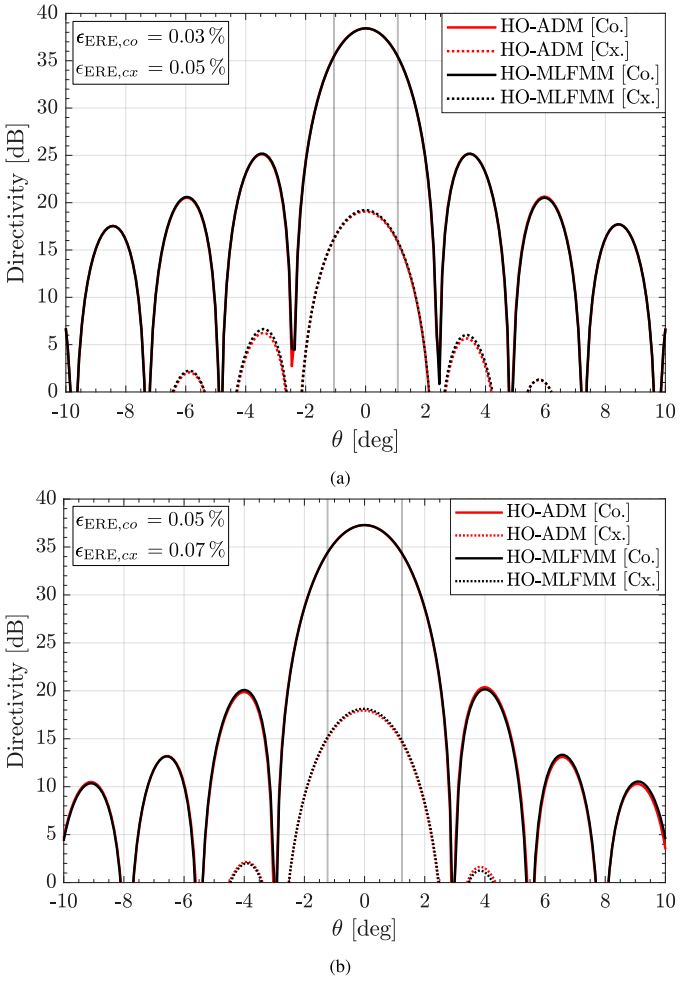

Fig. 9: Far-field directivity pattern ($\phi = 0°$-cut) at 8.4 GHz comparing the HO-ADM to the HO-MLFMM for (a) the antenna of Fig. 8a (b) the thinned array of Fig. 8b. Co-polarization is RHCP whereas the cross-polarization is LHCP. 3.0 dB-beamwidths are marked with dark-gray vertical lines.

putational complexity scaling in s (number of basis functions per array element), which impacts both the memory $\mathcal{O}(s^2T)$ and computational complexity $\mathcal{O}(s^2T \log T)$ for HO-ADM. Here it should be noted that the asymptotic total computational complexity and memory scaling of MLFMM is $\mathcal{O}(sT \log sT)$. For a fixed array element discretization, s can be considered constant, hence the memory consumption of HO-ADM will become smaller than that of HO-MLFMM for larger arrays.

While the computational complexity remains the same between HO-ADM and HO-MLFMM, they differ significantly in their respective computational complexity constants. The break-even value of s is strongly problem-dependent; that is, it varies significantly with the complexity of the individual elements and how many array elements are considered. From our investigations, we found that the asymptotic break-even point, s_∞ for $T \to \infty$ (infinite number of array elements) is on average in the order of 4000 but can vary from 1000 to 10000 and even higher.

C. Circular Rim Patch Antenna Array

The third example takes outset in the same 32×32-element array but assuming it needs to conform to a circular rim. To this end, the antenna array needs to be thinned which is achieved in HO-ADM as described in Section III-A. The resulting 793-element array is depicted in Fig. 8b, and is meshed with a total of 92,323 quadrilaterals comprising $N = 755{,}370$ unknowns in the HO-MLFMM, whereas 18,312 (2.4 %) additional unknowns are needed in the HO-ADM due to the DGM and dummy unknowns.

The radiated far-field pattern has been computed at 8.4 GHz and is shown in Fig. 9b with an equivalent relative error of 0.05 % and 0.07 % for co-pol and cx-pol, respectively. As anticipated for a smaller aperture, the peak-directivity is 1.1 dB smaller at 37.3 dB, and the first side-lobe level at 19.9 dB is close to a uniformly excited circular aperture. The 3 dB beamwidth is only 0.2° larger for the thinned array compared to the full 32×32 array.

Solution time and memory consumption in the case of the circular-thinned antenna array can be found in Table II enclosed in parentheses. Whereas the HO-MLFMM uses 57 min, the total solution time for the HO-ADM in case of the thinned array is unaltered at 6 min and 18 s. Firstly, this is because all matrix blocks $\mathbf{a}_{k,l}$ need to be computed and stored in the HO-ADM regardless of the number of thinned elements in the array. Secondly, for this particular case, the slightly faster MVP compensates for the additional iterations which are needed due to the employed preconditioner being less effective for the circular-thinned array.

V. Conclusion

We presented two extensions to the Higher-Order Array Decomposition Method enabling it to handle thinned and connected arrays of antennas or scatterers. The Discontinuous Galerkin Method (DGM) for surface integral equations has been employed together with appropriately placed dummy unknowns to retain the FFT-accelerated matrix-vector product even for connected arrays.

The presented method significantly reduces the solution time by more than an order of magnitude for both a 32×32-element square array and a 793-element circular-thinned array. This improvement in speed is achieved without approximations and without significantly increasing memory consumption compared to existing fast methods like the MLFMM.

We note that future work includes an extension to the presented method enabling the simulation of non-identical array elements, by exploiting the same technique as described in Section III-A.

Acknowledgment

The authors would like to thank the anonymous reviewers for their valuable comments and suggestions.

References

[1] R. Coifman, V. Rokhlin, and S. Wandzura, "The fast multipole method for the wave equation: A pedestrian prescription," *IEEE Antennas and Propagation Magazine*, vol. 35, no. 3, pp. 7–12, 1993.

[2] C.-C. Lu and W. C. Chew, "A multilevel algorithm for solving a boundary integral equation of wave scattering," *Microwave and Optical Technology Letters*, vol. 7, no. 10, pp. 466–470, 1994.

[3] J. Song, C.-C. Lu, and W. C. Chew, "Multilevel fast multipole algorithm for electromagnetic scattering by large complex objects," *IEEE Transactions on Antennas and Propagation*, vol. 45, no. 10, pp. 1488–1493, 1997.

[4] X. Zhao, Z. Lin, Y. Zhang, S.-W. Ting, and T. K. Sarkar, "Parallel hybrid method of HOMoM–MLFMA for analysis of large antenna arrays on an electrically large platform," *IEEE Transactions on Antennas and Propagation*, vol. 64, no. 12, pp. 5501–5506, 2016.

[5] B. Karaosmanoğlu and Ö. Ergül, "Acceleration of MLFMA simulations using trimmed tree structures," *IEEE Transactions on Antennas and Propagation*, vol. 69, no. 1, pp. 356–365, 2020.

[6] W. B. Lu, T. J. Cui, and H. Zhao, "Acceleration of fast multipole method for large-scale periodic structures with finite sizes using sub-entire-domain basis functions," *IEEE Transactions on Antennas and Propagation*, vol. 55, no. 2, pp. 414–421, 2007.

[7] V. Prakash, , and R. Mittra, "Characteristic basis function method: A new technique for efficient solution of method of moments matrix equations," *Microwave and Optical Technology Letters*, vol. 36, no. 2, pp. 95–100, 2003.

[8] E. Lucente, A. Monorchio, and R. Mittra, "An iteration-free MoM approach based on excitation independent characteristic basis functions for solving large multiscale electromagnetic scattering problems," *IEEE Transactions on Antennas and Propagation*, vol. 56, no. 4, pp. 999–1007, 2008.

[9] L. Matekovits, V. A. Laza, and G. Vecchi, "Analysis of large complex structures with the synthetic-functions approach," *IEEE Transactions on Antennas and Propagation*, vol. 55, no. 9, pp. 2509–2521, 2007.

[10] W. Xiang, W. Yang, and W. Lu, "Fast sub-entire-domain basis functions method for analysis of composite finite periodic structures with dielectric-conductor cells," *IEEE Antennas and Wireless Propagation Letters*, 2022.

[11] S. Kapur and D. E. Long, "IES3: a fast integral equation solver for efficient 3-dimensional extraction." in *ICCAD*, vol. 97, 1997, pp. 448–455.

[12] S. M. Seo and J.-F. Lee, "A single-level low rank IE-QR algorithm for PEC scattering problems using EFIE formulation," *IEEE Transactions on Antennas and Propagation*, vol. 52, no. 8, pp. 2141–2146, 2004.

[13] S. Kurz, O. Rain, and S. Rjasanow, "The adaptive cross-approximation technique for the 3d boundary-element method," *IEEE Transactions on Magnetics*, vol. 38, no. 2, pp. 421–424, 2002.

[14] Q. Gueuning, E. D. L. Acedo, A. K. Brown, and C. Craeye, "An inhomogeneous plane-wave based single-level fast direct solver for the scattering analysis of extremely large antenna arrays," *IEEE Transactions on Antennas and Propagation*, 2022.

[15] W. Yu, H. Yang, S. Li, and Y. Xu, "An HSS-matrix-based fast direct solver with randomized algorithm," *The Applied Computational Electromagnetics Society Journal*, pp. 814–817, 2018.

[16] E. Bleszynski, M. Bleszynski, and T. Jaroszewicz, "AIM: Adaptive integral method for solving large-scale electromagnetic scattering and radiation problems," *Radio Science*, vol. 31, no. 5, pp. 1225–1251, 1996.

[17] S. Sharma and P. Triverio, "AIMx: an extended adaptive integral method for the fast electromagnetic modeling of complex structures," *IEEE Transactions on Antennas and Propagation*, vol. 69, no. 12, pp. 8603–8617, 2021.

[18] J. White, J. Phillips, and T. Korsmeyer, "Comparing precorrected-FFT and fast multipole algorithms for solving three-dimensional potential integral equations,"," in *Proceedings of the Colorado Conference on Iterative Methods*. Citeseer, 1994, pp. 4–10.

[19] S. M. Seo and J.-F. Lee, "A fast IE-FFT algorithm for solving PEC scattering problems," *IEEE Transactions on Magnetics*, vol. 41, no. 5, pp. 1476–1479, 2005.

[20] S.-C. Lee, M. N. Vouvakis, and J.-F. Lee, "A non-overlapping domain decomposition method with non-matching grids for modeling large finite antenna arrays," *Journal of Computational Physics*, vol. 203, no. 1, pp. 1–21, 2005.

[21] Z. Peng, X.-C. Wang, and J.-F. Lee, "Integral equation based domain decomposition method for solving electromagnetic wave scattering from non-penetrable objects," *IEEE Transactions on Antennas and Propagation*, vol. 59, no. 9, pp. 3328–3338, 2011.

[22] R. W. Kindt, K. Sertel, E. Topsakal, and J. L. Volakis, "Array decomposition method for the accurate analysis of finite arrays," *IEEE Transactions on Antennas and Propagation*, vol. 51, no. 6, pp. 1364–1372, 2003.

[23] E. H. Bleszynski, M. K. Bleszynski, and T. Jaroszewicz, "Block-Toeplitz fast integral equation solver for large finite periodic and partially periodic array systems," *IEICE Transactions on Electronics*, vol. 87, no. 9, pp. 1586–1594, 2004.

[24] R. W. Kindt and J. L. Volakis, "Array decomposition-fast multipole method for finite array analysis," *Radio Science*, vol. 39, no. 2, pp. 1–9, 2004.

[25] M. Brandt-Møller, M. Mattes, O. Breinbjerg, M. Zhou, and O. Borries, "Array decomposition method for arbitrary-element regular arrays using higher-order basis functions," *IEEE Antennas and Wireless Propagation Letters*, 2022.

[26] E. Jørgensen, J. L. Volakis, P. Meincke, and O. Breinbjerg, "Higher order hierarchical Legendre basis functions for electromagnetic modeling," *IEEE Transactions on Antennas and Propagation*, vol. 52, no. 11, pp. 2985–2995, 2004.

[27] R. D. Graglia, D. R. Wilton, and A. F. Peterson, "Higher order interpolatory vector bases for computational electromagnetics," *IEEE Transactions on Antennas and Propagation*, vol. 45, no. 3, pp. 329–342, 1997.

[28] E. Jørgensen, *Higher-order integral equation methods in computational electromagnetics*. Ørsted-DTU, PhD Dissertation, 2003.

[29] G. H. Golub and C. F. Van Loan, *Matrix computations*. JHU Press, 1996.

[30] "IEEE standard for definitions of terms for antennas," pp. ix+38, 2014.

[31] Z. Peng, K.-H. Lim, and J.-F. Lee, "A discontinuous Galerkin surface integral equation method for electromagnetic wave scattering from non-penetrable targets," *IEEE Transactions on Antennas and Propagation*, vol. 61, no. 7, pp. 3617–3628, 2013.

[32] Z. Peng, R. Hiptmair, Y. Shao, and B. MacKie-Mason, "Domain decomposition preconditioning for surface integral equations in solving challenging electromagnetic scattering problems," *IEEE Transactions on Antennas and Propagation*, vol. 64, no. 1, pp. 210–223, 2015.

[33] X.-W. Huang, M.-L. Yang, and X.-Q. Sheng, "A simplified discontinuous Galerkin self-dual integral equation formulation for electromagnetic scattering from extremely large IBC objects," *IEEE Transactions on Antennas and Propagation*, vol. 70, no. 5, pp. 3575–3586, 2021.

[34] V. F. Martin, D. M. Solis, M. G. Araujo, L. Landesa, F. Obelleiro, and J. M. Taboada, "A discontinuous galerkin integral equation approach for electromagnetic modeling of realistic and complex radiating systems," *IEEE Transactions on Antennas and Propagation*, pp. 1–1, 2023.

[35] B.-B. Kong and X.-Q. Sheng, "A discontinuous Galerkin surface integral equation method for scattering from multiscale homogeneous objects," *IEEE Transactions on Antennas and Propagation*, vol. 66, no. 4, pp. 1937–1946, 2018.

[36] V. F. Martín, L. Landesa, F. Obelleiro, and J. M. Taboada, "A discontinuous Galerkin combined field integral equation formulation for electromagnetic modeling of piecewise homogeneous objects of arbitrary shape," *IEEE Transactions on Antennas and Propagation*, vol. 70, no. 1, pp. 487–498, 2021.

[37] TICRA, "TICRA Tools ESTEAM," https://www.ticra.com/software/esteam/, 2019.

[38] O. Borries, P. Meincke, E. Jørgensen, S. B. Sørensen, and P. C. Hansen, "Improved multilevel fast multipole method for higher-order discretizations," *European Conference on Antennas and Propagation*, pp. 3610–3614, 2014.

[39] N. Chahat, B. Cook, H. Lim, and P. Estabrook, "All-metal dual-frequency RHCP high-gain antenna for a potential europa lander," *IEEE Transactions on Antennas and Propagation*, vol. 66, no. 12, pp. 6791–6798, 2018.

Magnus Brandt-Møller was born in Hvidovre, Denmark, in 1995. He received the B.Sc. and M.Sc. degrees in electrical engineering from the Technical University of Denmark (DTU), Lyngby, in 2017 and 2020, respectively. He is currently pursuing the Ph.D. degree at the Technical University of Denmark, focusing on the full-wave numerical modeling of electrically large finite-array structures. His research interest include computational electromagnetics, antenna theory, and analysis and design techniques for phased array antennas.

Michael Mattes (M'08) received the Dipl-Ing. degree from the University of Ulm, Ulm, Germany, in 1996, and the Dr és science degree from the Ecole Polytechnique Fédérale de Lausanne (EPFL), Lausanne, Switzerland, in 2003. After a one-year Research Fellowship at the Department of Microwave Techniques, University of Ulm, he joined the Laboratory of Electromagnetism and Acoustics (LEMA), EPFL, in September 1997. From 2003 until 2016, he has held a permanent Research Fellow and Lecturer position at EPFL. In 2016, he has been appointed Associate Professor at the Electrical Engineering Department of the Technical University of Denmark (DTU). His research interests include electromagnetic theory, numerical methods, and direct and inverse scattering problems.

Olav Breinbjerg (M'87, S'16, F'19) was born in Silkeborg, Denmark, in 1961. He received the M.Sc. and Ph.D. degrees in electrical engineering from the Technical University of Denmark (DTU) in 1987 and 1992, respectively. He was on the Faculty of the Department of Electrical Engineering as an Assistant Professor from 1991 to 1995, Associate Professor from 1995 to 2005, and Full Professor from 2006 to 2021; from 1997 to 2021 he was also Head of the Electromagnetic Systems Group and the DTU-ESA Spherical Near-Field Antenna Test Facility. He resigned his position at DTU in May 2021 and is now an independent consultant. Olav Breinbjerg was a Visiting Scientist at Rome Laboratory in 1988, a Fulbright Research Scholar at the University of Texas at Austin in 1995, and a Visiting Professor at the University of Sienna in 2011 and 2022. He has been the main supervisor of 17 Ph.D. students. His research is generally in applied electromagnetics— and particularly in antennas, antenna measurements, computational techniques, and scattering—for applications in wireless communication and sensing technologies. He is the author or co-author of more than 60 journal papers, 250 conference papers, and 250 technical reports. Dr. Breinbjerg was a recipient of a U.S. Fulbright Research Award in 1995, the 2001 AEG Elektron Foundation's Award, the 2003 DTU Student Union's Teacher of the Year Award, the 2013 and 2015 European School of Antennas Teacher of the Year Awards, and the 2020 Hans Christian Ørsted Award. He is Fellow of AMTA and IEEE.

Min Zhou (S'12–M'13) was born in 1984 in Beijing, China. He received the M.Sc. degree in electrical engineering from the Technical University of Denmark (DTU), Lyngby, Denmark, in 2009, and the Ph.D. degree in 2013 at the same university. Since 2009, he has been with the Danish company TICRA, Copenhagen, Denmark, where he is working with the development of commercial software for antenna analysis and design. His research interest include computational electromagnetics, antenna theory, and analysis and design techniques for quasi-periodic surfaces such as reflectarrays and frequency selective surfaces. M. Zhou received DTU's Young Researcher Award for his Ph.D. work on reflectarrays in 2013. He was also the recipient of the Best Innovative Paper Award at the 36th and 40th ESA Antenna Workshop in 2015 and 2019, respectively.

Erik Jørgensen (M'03) was born in 1974 in Denmark. He received the M.Sc. and Ph.D. degrees in electrical engineering from the Technical University of Denmark (DTU), in 2000 and 2003, respectively. In 1998, he was a visiting scholar at the University of Siena, Italy, and in 2001, he spent half a year at the Radiation Laboratory, University of Michigan, Ann Arbor, Michigan. Since 2003, Erik Jørgensen has been with the Danish company TICRA, Copenhagen, where he has held multiple managerial positions while being involved in the development of commercial antenna modeling tools. His research interests include integral equations, higher-order methods, high-frequency methods, and computational electromagnetics in general.